

Grazing-incidence x-ray scattering from stepped interfaces in AlAs/GaAs superlattices

E. A. Kondrashkina,* S. A. Stepanov,* R. Opitz, M. Schmidbauer, and R. Köhler
AG Röntgenbeugung, Humboldt-Universität zu Berlin, Hausvogteiplatz 5-7, Berlin D-10117, Germany

R. Hey and M. Wassermeier
Paul-Drude-Institut für Festkörperelektronik, Hausvogteiplatz 5-7, Berlin D-10117, Germany

D. V. Novikov
HASYLAB am DESY, Notkestraße 85, Hamburg D-22603, Germany
 (Received 14 March 1997; revised manuscript received 3 July 1997)

The features of surface and interface roughness in crystalline AlAs/GaAs superlattices grown by molecular beam epitaxy on vicinal (001) GaAs substrates are studied by grazing-incidence x-ray scattering (GIXS). The effects of different growth modes [step-flow or two-dimensional- (2D-) nucleation], different substrate preparations, and growth interruptions on the roughness are investigated. The results of GIXS are compared with atomic force microscopy (AFM) images of sample surfaces. For samples grown in the step-flow mode, both of the methods display a distinct anisotropy in the lateral size of roughness along the substrate miscut direction and perpendicular to it. The lateral correlation lengths given by GIXS correspond to the size of step bunches observed by AFM, while individual steps are resolved by AFM only. GIXS reveals also a strong interface-interface correlation or inheritance of roughness for all the samples which is not accessible by AFM. Moreover, the angle of inclination of the direction of this inheritance from the surface normal is found to be dependent on the growth conditions. Two effects in the skew inheritance have been observed by means of 2D mapping of GIXS in the reciprocal space: (i) in the direction of substrate miscut the angle of skew inheritance inverted its sign, (ii) in the direction perpendicular to the miscut a strongly skew inheritance appeared as an effect of growth interruptions. Conclusions concerning the improvement of GIXS experiments applied to the studies of multilayers are derived. [S0163-1829(97)04839-X]

I. INTRODUCTION

Interfaces in semiconductor multilayers are of a wide practical interest since their quality directly affects the operation of microelectronic devices. However, many methods of material science, like atomic force microscopy (AFM), reflection electron microscopy, or reflection high-energy electron diffraction (RHEED) probe the sample surface roughness only, providing no information about internal interfaces. In the recent years nonspecular grazing-incidence x-ray scattering (GIXS) has proved to be a powerful tool for studying roughness phenomena, since it can deliver statistically averaged information about roughnesses of buried interfaces and their correlations in multilayers.¹⁻³⁰

Originally, GIXS method was developed for characterization of the roughness of amorphous samples.¹ Later on, it was also applied to crystalline multilayers,^{4,7,9,10,14-16,21-23,25-30} and some of these applications revealed effects not observed for amorphous objects. Among these are a difference between GIXS measured along the surface miscut direction and perpendicular to it,^{10,14,16,21,27-29} an asymmetry of the GIXS pattern along the miscut direction,^{10,16,21,28,29} and the formation of periodic peaks in transverse scans of GIXS.^{4,10,21,29} These are clear indications of specific features of roughness in multilayers, like atomic steps on vicinal interfaces,^{4,10,14} strain relaxation,²⁹ or skew roughness transfer between interfaces.^{16,28} However, the relationship between GIXS patterns and interface morphology in crystals is still under

discussion.¹⁶ It is not completely understood as yet, how the surface and interface morphology develops and how it is inherited from interface to interface. In the case of strongly strained layer systems it has been suggested that the inheritance of the morphology is of thermodynamic rather than kinetic origin.¹⁶ Such a mechanism is, however, not expected to be effective for weakly strained systems like AlAs/GaAs. Here the surface morphology is dominated by step bunching (at least in the step-flow growth mode) which is mainly influenced by growth kinetics. The direction of inheritance strongly deviates from the surface normal and behaves in a peculiar way depending on the growth conditions.²⁸ The above phenomena urgently require detailed experimental and theoretical investigations.

In Sec. II we give a summary of the theory used for the analysis of GIXS from crystalline multilayers. Special attention is paid to the effect of steps on vicinal surfaces and of a skew roughness transfer in multilayers on GIXS.

In Sec. III the details of the sample preparation and the experimental techniques are described. Unlike most of the previous studies we applied a 2D mapping of GIXS in reciprocal space. This enabled us to reveal several new effects which, to our knowledge, had not been noticed before. AFM was also used in this study. The results obtained by both methods are described in Sec. IV and compared and discussed in Sec. V. We conclude with a summary of experimental evidence and some recommendations regarding an improvement of GIXS techniques applied to semiconductor multilayers and other crystals.

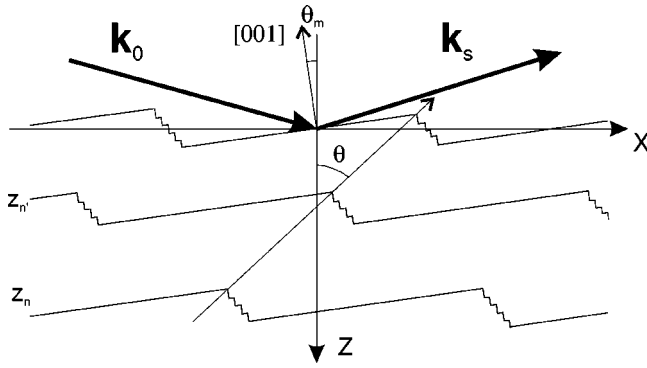


FIG. 1. Effects causing the asymmetry of grazing-incidence x-ray scattering from multilayers: (i) steps at vicinal interfaces due to a small misorientation angle θ_m between interfaces and a crystallographic plane and (ii) the skew inheritance of interfacial roughness by the angle θ . The other notations are \mathbf{k}_0 , \mathbf{k}_s —wave vectors of incident and scattered waves respectively, X —direction along sample surface, Z —internal surface normal. For clarity, the vertical scale is expanded relative to the horizontal scale.

II. THEORY

Nonspecular x-ray scattering from rough interfaces is caused by the fluctuations $\Delta\chi(\mathbf{r})$ of material susceptibility in the scattering object when material A forming the interface occurs in the place of material B and vice versa. The most commonly used approach to calculate this effect in the lowest order over the perturbation $\Delta\chi(\mathbf{r})$ is to apply the distorted wave Born approximation (DWBA).^{1,2,12,13,15,18,20} The general expression for the cross section of nonspecular x-ray scattering from a multilayer with N nonflat interfaces is

$$\frac{d\sigma}{d\Omega} = \frac{S\kappa^4}{16\pi^2} \sum_{n,n'=1}^N \sum_{i,i'=r,t} \sum_{j,j'=r,t} \frac{C_{nij}C_{n'i'j'}^*}{q_{znij}q_{zn'i'j'}^*} \times \int d^2\rho [e^{iq_{znij}q_{zn'i'j'}^*K_{nn'}(\rho)} - 1]e^{-iq_{\parallel}\rho}. \quad (1)$$

Here

$$C_{nij} = \Delta\chi_0^n D_{ni}^{\text{in}} D_{nj}^{\text{out}} e^{iq_{znij}z_n - \sigma_n^2 q_{znij}^2/2}, \quad (2)$$

the parameters $\Delta\chi_0^n$ are the differences in the mean x-ray susceptibilities of the two layers forming the n th interface; S is the illuminated sample surface area; $\mathbf{q}_{nij} = \mathbf{k}_{ni}^{\text{in}} + \mathbf{k}_{nj}^{\text{out}}$ is the momentum transfer at scattering; and indices z and \parallel denote the vector components perpendicular and along the surface, respectively. Finally, $\mathbf{k}_{ni}^{\text{in,out}}$ and $D_{ni}^{\text{in,out}}$ are the wave vectors and the amplitudes, respectively, of transmitted (t) and reflected (r) waves which are the solution to the specular reflection problem in multilayers for the real incident wave \mathbf{k}_0 (denoted as “in”) and a virtual incident wave (“out”) which is the inverted scattered wave \mathbf{k}_s (see Fig. 1). Both the “in” and the “out” solutions correspond to flat interfaces and can be given by the Parratt or Abeles methods.^{31,32} The parameters $\sigma_n^2 = \langle \delta z_n^2(0) \rangle$, and $K_{nn'}(\rho) = \langle \delta z_n(0) \delta z_{n'}(\rho) \rangle$ are the rms roughness and the correlation function of the interface relief, respectively.

We consider the most widely used GIXS experiments where the scattered waves are analyzed as a function of their

takeoff angle to the surface and integrated over their deviations from the incidence plane. Then Eq. (1) is integrated over the component q_y of the momentum transfer which is perpendicular to the incidence plane:

$$\frac{d\sigma}{d\Omega} = \frac{S\kappa^3}{8\pi} \sum_{n,n'=1}^N \sum_{i,i'=r,t} \sum_{j,j'=r,t} \frac{C_{nij}C_{n'i'j'}^*}{q_{znij}q_{zn'i'j'}^*} \times \int_{-\infty}^{+\infty} dx [e^{q_{znij}q_{zn'i'j'}^*K_{nn'}(x)} - 1]e^{-iq_x x}. \quad (3)$$

As given by Eq. (3), an asymmetry of the GIXS pattern with respect to $\pm q_x$ may appear solely due to an asymmetry in the correlation function $K_{nn'}(x)$ of the interface morphology *in the plane of incidence*. For self-affine roughness which is characteristic to amorphous materials the correlation function $K_{nn'}(x)$ depends only on the distance $|x|$ between the two points. Thus, the GIXS pattern is always symmetric.

As reported by several groups,^{10,14,16,21} x-ray scattering from crystalline multilayers can exhibit (a) anisotropy and (b) asymmetry (polarity). These results were observed for vicinal surfaces with a small miscut angle $\theta_m \lesssim 1^\circ$ from a crystallographic plane. Interfaces of multilayers grown on such surfaces are not flat and consist of atomic steps and step bunches.³³

The observed anisotropy was the difference between GIXS patterns taken with the incidence plane of x rays being parallel and perpendicular to steps.^{10,14,16,21} The asymmetry (polarity) was observed when the plane of x-ray incidence was directed along the miscut and crossed the steps. Then, the GIXS pattern became asymmetric with respect to the right and left x-ray momentum transfers q_x along the interfaces. When the plane of incidence was rotated by 180° , the asymmetry of GIXS was inverted and one could speak about polarity in this sense. This effect was observed for Si/Ge superlattices.^{10,16,21}

The anisotropy effect does not require any special theory since GIXS experiments probe interface morphology in the incidence plane only. That means, the models of scattering from isotropic roughness developed for amorphous objects are applicable for each particular measurement. Contrary to that, the asymmetry effect is an indication of an asymmetry in the correlation function. Thus, the derivation of asymmetric $K_{nn'}(x)$ is the major aim of this section. Two different kinds of asymmetry can be assumed.

A. Skew roughness inheritance

First, a skew inheritance of interface morphology might take place at multilayer growth, i.e., the roughness features of the bottom interface are inherited by succeeding interfaces at some angle θ to the interface normal (Fig. 1). For instance, the inheritance might be declined from the surface normal towards the step-flow direction, as observed in Ref. 16 and shown in Fig. 1. The inheritance along some crystallographic axis might also become favorable.

In the case of the skew roughness transfer the interface-interface correlation function transforms as

$\mathcal{K}_{nn'}(x) \rightarrow \mathcal{K}_{nn'}[x - \tan\theta(z_n - z_{n'})]$, where z_n are the coordinates of interfaces (see Fig. 1). With this function Eq. (3) takes the form

$$\frac{d\sigma}{d\Omega} = \frac{S\kappa^3}{8\pi} \sum_{n,n'} \sum_{i,i'} \sum_{j,j'} \frac{C_{nij}C_{n'i'j'}^*}{q_{znij}q_{zn'i'j'}^*} e^{-iq_x \tan\theta(z_n - z_{n'})} \times \int_{-\infty}^{+\infty} dx [e^{q_{znij}q_{zn'i'j'}^* \mathcal{K}_{nn'}(x)} - 1] e^{-iq_x x}, \quad (4)$$

and the factor $\exp[-iq_x \tan\theta(z_n - z_{n'})]$ in Eq. (4) provides the asymmetry of GIXS with respect to $\pm q_x$. Equation (4) is symmetric at $q_x = 0$ and the asymmetry increases with $|q_x|$. In the case of a periodic multilayer with correlated interface roughness where x-ray scattering is bunched into resonance diffuse scattering (RDS) sheets parallel to q_x axis and perpendicular to the specular rod,^{15,20} the skew roughness transfer causes a tilt of the sheets by the angle θ around their centers at the specular rod. In most of GIXS experiments $q_x \ll q_z$, and therefore only large angles $\theta \gtrsim 1$ rad can be detected. Therefore, for example, GIXS cannot resolve whether roughness is transferred along the surface normal, or along the normal to a vicinal crystallographic plane, since the angle between them is small. The larger transfer angles which could be resolved might appear in step-flow grown samples, or if the roughness were inherited in some other crystallographic direction.

The numerical examples are not given here, because a lot of them will be presented in the experimental part. For $\mathcal{K}_{nn'}(x)$ we used the self-affine roughness model by Sinha *et al.*¹ and the interface-interface correlations in the form by Ming *et al.*:⁹

$$\mathcal{K}_{nn'}(x) = \sigma^2 \exp[-(x/\xi)^{2h}] \exp(-|z_n - z_{n'}|/\xi_z). \quad (5)$$

Here h is a roughness exponent ($0 < h < 1$), determining ‘‘jaggedness’’ of roughness, ξ is the lateral correlation length corresponding to a characteristic lateral size of roughness, and ξ_z is the vertical correlation length for interface-interface roughness correlations. At $\xi_z = \infty$ all the interfacial reliefs are completely correlated (replicated) and at $\xi_z = 0$ they are non-correlated. Equation (5) neglects a different vertical correlation for roughness with small and great lateral size,^{11,20} but it does account for strong correlations observed in our experiment. The advantage of this function is that it makes calculations fast.

B. Asymmetric scattering from atomic steps

Another possible source of the asymmetry of GIXS is the atomic steps on vicinal interfaces of crystals (see Fig. 1). Since vicinal interfaces look different when they are illuminated from the left and right sides, GIXS patterns can be different too. The scattering from stepped surfaces was widely discussed for RHEED.³⁷⁻⁴¹ Some of these results have been used for x-ray scattering,^{4,10} however, without detailed analysis. Alternatively, a study by Sinha *et al.*¹⁴ predicted that (i) x-ray scattering from stepped interfaces peaks in the reciprocal space along the line $q_x = -q_z \theta_m$, which is perpendicular to the surfaces of terraces between steps (to vicinal crystallographic plane), and (ii) the GIXS pattern at small $q_x \xi \ll 1$ would be symmetric and given by a self-affine

model of interface roughness. Indeed, an additional non-specular x-ray reflection peak at angle θ_m was found in Ref. 42 for *agglomerated* facets on carefully prepared stepped surfaces.

Our further consideration is confined to small roughness, where $q_z \sigma \ll 1$. Then, Eq. (3) reduces to

$$\frac{d\sigma}{d\Omega} = \frac{S\kappa^3}{8\pi} \sum_{n,n'} \sum_{i,i'} \sum_{j,j'} C_{nij}C_{n'i'j'}^* \mathcal{K}_{nn'}(q_x), \quad (6)$$

where $\mathcal{K}_{nn'}(q_x) = \int dx \mathcal{K}_{nn'}(x) \exp(-iq_x x)$ is a Fourier transform of the correlation function. In addition, we assume that the incidence and exit angles of x rays are larger than the critical angle for total external reflection, so that x-ray specular reflection and refraction effects can be neglected. Then, we can put $D_{nr}^{\text{in,out}} = 1$, $D_{nr}^{\text{in,out}} = 0$, $q_{znti} \equiv q_z$, and Eq. (6) further reduces to the Born approximation:

$$\frac{d\sigma}{d\Omega} = \frac{S\kappa^3}{8\pi} \sum_{n,n'} \Delta \chi_0^n (\Delta \chi_0^{n'})^* e^{-q_z^2 (\sigma_n^2 + \sigma_{n'}^2)/2} \times e^{iq_z(z_n - z_{n'})} \mathcal{K}_{nn'}(q_x). \quad (7)$$

Under the above simplifications, the correlation function $\mathcal{K}_{nn'}(q_x)$ can be taken in the forms obtained in Refs. 14 and 39 for x-ray scattering and RHEED from stepped interfaces, respectively. The result of Ref. 14 is difficult for analysis, since it is expressed in terms of an infinite series of the correlation functions of individual steps. Therefore, we take the correlation function from Ref. 39, where a sum of the series was found in a compact form. Some of previous GIXS studies used this function too.^{4,10} After a few transformations the result of Ref. 39 can be presented as

$$\mathcal{K}_{nn'}(q_x) = \frac{2A_{nn'}}{q_x^2 \xi} \text{Re} \frac{[1 - P(q_x)][1 - H(q_z)]}{1 - P(q_x)H(q_z)}, \quad (8)$$

$$P(q_x) = \int_0^\infty dL P(L) e^{-iq_x L}, \quad (9)$$

$$H(q_z) = \sum_{h=-\infty}^\infty H(h) e^{-iq_z h d}. \quad (10)$$

Here it is assumed that all interfaces have the same step distributions, and $A_{nn'}$ is a factor describing interface-interface correlations of steps, which will be determined later. The parameters d and $\xi \equiv \langle L \rangle$ are the elementary step height and the mean terrace length, respectively. $P(L)$ is a probability per unit length for a terrace of length L , and $H(h)$ is a probability for a step of height hd . These functions are normalized as

$$\int_0^\infty dL P(L) = 1, \quad \sum_{h=-\infty}^\infty H(h) = 1. \quad (11)$$

First, let us consider interfaces where all the steps are always in one direction and monoatomic. Then

$$H(h) = \delta_{h,1}, \quad H(q_z) = \exp(-iq_z d). \quad (12)$$

Assuming a geometric staircase, $P(L)$ and $P(q_x)$ can be presented as⁴⁵

$$P(L) = \xi^{-1} \exp(-L/\xi), \quad P(q_x) = 1/(1+iq_x\xi). \quad (13)$$

After the substitution of Eqs. (12) and (13) into Eq. (8) and on the assumption of small roughness ($q_z d \approx q_z \sigma \ll 1$), we obtain

$$\mathcal{K}_{nn'}^{\text{Mono}}(q_x) = \frac{A_{nn'} \xi q_z^2 d^2}{(q_x \xi + q_z d)^2 + q_z^4 d^4 / 4}. \quad (14)$$

The asymmetry of the GIXS pattern provided by the correlation function (14) is qualitatively different from that for skew roughness transfer. Here we have a shift of resonance sheets of GIXS towards negative q_x instead of their rotation given by Eq. (4). Thus, the two effects can be clearly distinguished.

Since $d = \theta_m \xi$, Eq. (14) provides a peak of x-ray scattering at $q_x = -q_z \theta_m$, i.e., along the normal to terrace surfaces. This coincides with the prediction by Sinha *et al.*¹⁴ and with the observation of peaks in GIXS from vicinal surfaces in Refs. 4, 10, and 42. However, there were no such peaks observed in some other experiments^{10,16,21} and in our own study. To explain this discrepancy, we have assumed that interfaces were not simple staircases and possessed random up and down fluctuations. Then, the correlation function may be viewed as a sum of a self-affine part due to fluctuations and the staircase part:

$$\mathcal{K}_{nn'}(q_x) = \mathcal{K}_{nn'}^{\text{Affine}}(q_x) + \mathcal{K}_{nn'}^{\text{Steps}}(q_x), \quad (15)$$

where, e.g., the Fourier-transform of the self-affine correlation function (5) presuming $h = 0.5$ is

$$\mathcal{K}_{nn'}^{\text{Ming}}(q_x) = \frac{2\xi\sigma^2}{(q_x\xi)^2 + 1} \exp(-|z_n - z_{n'}|/\xi_z). \quad (16)$$

Proceeding to a continuous step distribution, the probability distribution for step heights in the staircase part (8) can be presented as

$$H(q_z) = e^{-iq_z\theta_m\xi - q_z^2\sigma^2}, \quad (17)$$

where σ is the total rms roughness of interfaces and it is taken into account that the mean probability for steps to go up (down) on the lateral scale ξ must provide the interface shift in z direction by $\theta_m\xi$. Substituting Eq. (17) into Eq. (8) and assuming again a geometric staircase (13), we arrive at

$$\mathcal{K}_{nn'}^{\text{Steps}}(q_x) = \frac{2\xi\sigma_{\text{eff}}^2 q_z^2 A_{nn'}}{(q_x\xi + q_z\theta_m\xi)^2 + q_z^4\sigma_{\text{eff}}^4}, \quad (18)$$

where $\sigma_{\text{eff}}^2 = \sigma^2 + \theta_m^2 \xi^2 / 2$. If the fluctuations at the interfaces are high, then $\sigma^2 \gg \theta_m^2 \xi^2$, and the peak given by Eq. (18) is much broader than that given by Eq. (14). In the range of small q_x it appears as an asymmetry of the GIXS pattern only.

At small $q_x \xi \ll 1$ Eqs. (18) and (16) possess a similar structure, thus confirming the statement by Sinha *et al.*¹⁴ that the self-affine model of interface roughness can be applicable to GIXS from stepped interfaces at small q_x . Taking into

account the similarity of the correlation functions, the factor $A_{nn'}$ is chosen in the form $A_{nn'} \approx \sigma_s^2 \exp(-|z_n - z_{n'}|/\xi_z)$, where σ_s^2 is a fitting parameter corresponding to an effective rms roughness of interfaces caused by atomic staircases.

C. Numerical procedures

Either of the above two models have been alternatively applied to the analysis of our experimental data. For the skew roughness transfer model, the calculations were performed using Eq. (4) with the correlation function in the form of Eq. (5). For the alternative assumption of stepped interfaces, Eq. (7) was used and the correlation function was taken as a sum (15) of the self-affine (5) and the smoothed steps (18) contributions, respectively, in order to smear the peak along $q_x = -q_z \theta_m$ given by the steps model and not observed in our experiment.

Since the two models provide the two qualitatively different types of GIXS patterns discussed above, we were able to distinguish between them and it was found that our data were only explained by the skew roughness transfer. Therefore, all the calculations presented in the following sections are based on this model and here we discuss some details of the numerical procedures.

There is a practical problem that the computations with Eq. (4) are slow because it contains the six enclosed sums and the integral from the exponent, which in turn requires the expansion into the Taylor series.¹³ In view of the necessity to simulate the huge amount of data in our study, some additional simplifications were implemented without any substantial loss of precision.

First, we proceeded to the small-roughness approximation ($q_z \sigma \ll 1$), i.e., the integral in Eq. (4) was replaced by the Fourier transform of the correlation function like in Eq. (6). The latter one was tabulated once for different (q_x, h) and the tabulated values were used in the calculations of GIXS. The application of the above approximation to our case ($\sigma \approx 4$ Å) had a minor effect on the shape of the calculated GIXS patterns, which was the major parameter compared with experiment. The intensity calculated with this approximation was ~ 1.2 and ~ 1.8 times lower than that given by the original formula (4) for RDS-5 and RDS-8, respectively. However, that could be corrected.

Second, it was taken into account that the reflected amplitudes $D_{nr}^{\text{in,out}}$ are small outside the angular range for total external reflection. Therefore, the summation in Eq. (4) was restricted by the terms containing the transmitted amplitudes $D_{nt}^{\text{in,out}}$ only. This approximation is closer to the DWBA than the Born one [Eq. (7)], since it uses the amplitudes $D_{nt}^{\text{in,out}}$ given by the Parratt equations and containing all the refraction effects in the layers. With this approximation, even the Bragg-like peaks²⁰ in GIXS are perfectly reproduced (these are not seen on the patterns presented in Sec. IV because of averaging over the experimental resolution). Some deviations of this method from the DWBA are naturally observed for the Yoneda peaks at the critical angles for total external reflection. However, most of our experimental data went under the experimental background at the Yoneda peaks; in a few other cases the DWBA was applied.

Thus, the following formula was used in the majority of computations:

TABLE I. The structures and growth conditions of samples 1–4. The AlAs/GaAs superlattices are grown on vicinal GaAs substrates by molecular beam epitaxy. The surface miscut angles and directions are determined by x-ray diffraction. The buffer layer thicknesses are measured by *in situ* reflection high-energy electron diffraction. Buffer layer of sample 4 is grown as a single GaAs layer of 5000 Å and an additional 206 Å superlattice produced after 1800 s interruption and consisting of 16×4 ML GaAs and 5×2ML GaAs grown with 60 s interruptions. The parameters of superlattice samples are evaluated by simulating x-ray reflectivity curves. The surface rms roughness is measured by atomic force microscopy.

| Sample | 1 | 2 | 3 | 4 |
|--|-----------|--------------|---------------|------------|
| GaAs (001) substrate: | | | | |
| Surface miscut angle (°), ±0.03 | 0.38 | 0.40 | 0.43 | 0.38 |
| Deviation of miscut direction from (110) (°), ±5 | 8 | 5 | 0 | 6 |
| GaAs buffer layer thickness (Å) | 1000 | 1000 | 2000 | 5000 + 206 |
| Superlattice preparation: | | | | |
| Growth temperature (°C) | 610 | 610 | 580 | 610 |
| As ₄ /Ga beam equivalent pressure ratio | 12 | 15 | 17 | 7 |
| Growth rate (μm/h) | 0.5 | 0.5 | 0.5 | 0.5 |
| Growth mode of GaAs layers | step flow | transitional | 2D nucleation | step flow |
| Growth interruptions after GaAs (s) | | 120 | | 120 |
| Superlattice parameters: | | | | |
| Number of periods of AlAs/GaAs | 20 | 20 | 20 | 20 |
| AlAs layer thickness (Å), ±0.5 | 156.0 | 153.5 | 160.0 | 154.2 |
| GaAs layer thickness (Å), ±0.5 | 71.0 | 71.0 | 68.0 | 70.8 |
| Surface oxide thickness (Å), ±1 | 18 | 15 | 15 | 12 |
| Total rms roughness (Å), ±0.5 | 4.0 | 4.0 | 3.5 | 3.0 |
| Surface rms roughness (Å), ±0.2 | 4.2 | 4.7 | 3.3 | 2.3 |

$$\frac{d\sigma}{d\Omega} = \frac{S\kappa^3}{8\pi} \sum_{n,n'} C_{nnt} C_{n't't'}^* e^{-iq_x \tan\theta(z_n - z_{n'})} \mathcal{K}_{nn'}(q_x), \quad (19)$$

with $\mathcal{K}_{nn'}(q_x)$ being the Fourier transform of Eq. (5). The application of Eq. (19) provided about 30 times acceleration of calculations, as compared with Eq. (4).

III. EXPERIMENT

A. Sample preparation

Four model samples of AlAs/GaAs superlattice were grown by molecular beam epitaxy (MBE) on epi-ready GaAs (001) substrates. Some important parameters of the growth process are given in Table I.

In order to have similar initial stepped surfaces for the growth, vicinal GaAs substrates having the same small angle of surface miscut of $0.40^\circ \pm 0.03^\circ$ from the (001) plane into [110] direction were selected (as checked by x-ray diffraction). The deviation of surface miscut from [110] direction did not exceed 8° for all the substrates, see Table I.

Before the deposition of 20 period AlAs/GaAs superlattices GaAs buffer layers with different thicknesses (Table I) were grown. The conditions for superlattice growth, i.e., the As₄-to-Ga beam equivalent pressure ratio (BEP) and the growth temperature were chosen to provide different growth modes. The samples 1 and 4 were grown in the step-flow mode in the GaAs compound of the superlattice, whereas the growth mode of sample 3 was the 2D nucleation. The growth mode of sample 2 was probably at a transition from the step flow to 2D nucleation, due to a slightly increased BEP com-

pared to sample 1. An interruption of 120 s at the GaAs-to-AlAs interface was applied during the growth of samples 2 and 4.

B. Methods

GIXS measurements from the samples were performed using three different experimental setups. The first setup was a widely used conventional double-crystal diffractometer with a 1.5 kW x-ray tube, Ge(111) monochromator, slits on the incident beam side, and analyzing slit in front of scintillation detector. The adjustment of samples was implemented with the help of an analyzer crystal, which was removed at measurements to achieve a higher intensity. The setup allowed the measurements of both x-ray specular reflection and diffuse scattering with the resolutions of $\Delta q_z = 0.0036 \text{ \AA}^{-1}$ and $\Delta q_x = 0.0003 q_z$.

The second type of experimental setup included a 12 kW rotating anode (Rigaku), Ge(220) channel-cut monochromator, slits for the incident beam and a linear position sensitive detector, PSD (Braun), on the exit. The resolutions were $\Delta q_z = 0.0010 \text{ \AA}^{-1}$ and $\Delta q_x = 0.0002 q_z$. An advantage of this setup is the possibility of rapid mapping of x-ray scattering over a large area in the reciprocal space. However, there are some problems in the separation of high-intensive specular reflection and low-intensive diffuse scattering, which are discussed in Sec. IV.

The most precise measurements of GIXS were performed with synchrotron radiation at CEMO beamline of HASYLAB, DESY, Hamburg.⁴⁴ The setup included a double-crystal Si(111) monochromator, slits for the incident beam, and a Si(111) crystal analyzer in front of a scintillation

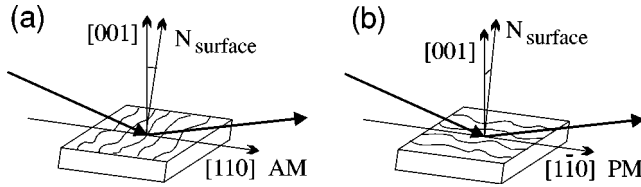


FIG. 2. Azimuthal orientation of the sample with respect to incident and exit x-ray waves when (a) x-ray scattering is measured along the surface miscut (AM) and step movement directions, and (b) perpendicular to miscut (PM). Vector N_{surface} denotes the external normal to the sample surface.

detector. The resolutions of $\Delta q_z = 0.0004 \text{ \AA}^{-1}$ and $\Delta q_x = 0.0001 q_z$ were achieved, which allowed the measurement of the intrinsic width of x-ray curves.

In the following sections these three experimental setups will be referred to as those with analyzing slit, with PSD and with crystal-analyzer, respectively.

In all the experimental schemes x rays with the wavelength of $\text{Cu } K_{\alpha 1}$ radiation were used. The resolution in q_y direction was restricted only by millimeter slits leading to an effective integration over q_y [see Eq. (3)]. Along with the mapping of GIXS over a large $q_x q_z$ area in the reciprocal space, single transverse q_x and longitudinal q_z scans were measured.

The x-ray measurements were performed in two directions $[110]$ and $[1\bar{1}0]$ for all the samples, i.e., along the direction of miscut and perpendicular to it. These directions are denoted in Fig. 2 as AM and PM, respectively. Some measurements for samples 1 and 2 were also taken in the opposite directions, $[\bar{1}\bar{1}0]$ and $[\bar{1}10]$, in order to verify that the peculiarities of curves and maps were not artificial.

In addition to the x-ray measurements, the surface morphology of the samples was imaged in real space by atomic force microscopy. A commercial ambient air atomic force microscope (Park Scientific Instruments) operating in constant force contact mode was used. The images were collected at a scan rate $10 \mu\text{m/s}$ and line-by-line corrected to account for the finite radius of curvature of the cylindrical piezos. The lateral and vertical resolution were 200 \AA and 0.2 \AA , respectively.

IV. RESULTS

A reciprocal space map of GIXS from sample 1 measured with PSD is shown in Fig. 3(a) as being typical for all the samples studied. The map exhibits a vertical streak of specular reflected intensity with superlattice Bragg peaks on it and a series of horizontal streaks corresponding to diffuse scattering concentrated into resonance diffuse scattering sheets.

The map in Fig. 3(a) consists of a series of PSD data lines which are directed diagonally and serially shifted in the vertical direction. Some of these data (the diagonal streaks marked by arrows) exhibit artifacts occurring when the PSD was oversaturated by a high intensity in the low-order superlattice Bragg peaks. Then, the signal spreaded over the other PSD channels producing the artificial strip. These artifacts can be partially suppressed by using a wirelike attenuator in front of those PSD channels which record the specularly reflected beam.

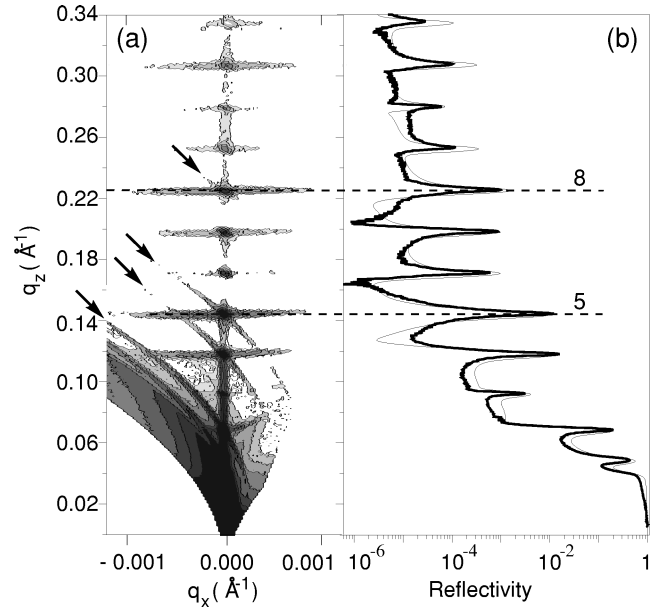


FIG. 3. Reciprocal space map of GIXS from sample 1, (a) and specular reflection curve corresponding to q_z section of the map at $q_x=0$, (b). The fifth and eighth RDS sheets are marked by numbers 5 and 8, respectively. Arrows indicate artifacts due to PSD crosstalk.

The specular reflection curve corresponding to the q_z section of the map at $q_x=0$ is shown in Fig. 3(b). It exhibits the same set of superlattice Bragg peaks and a long hump of intensity due to a surface oxide layer. The mean slope of the curve with q_z is determined by the average roughness of the surface and all interfaces. The thin line in Fig. 3(b) shows a simulated curve calculated by the Parratt's method³¹ with regard to roughness. Fitted parameters of the superlattices such as the thicknesses of the AlAs and GaAs layers within one period, the thickness of surface oxide layer, and the total root mean square (rms) roughness of the surface and the interfaces are listed in Table I for all the samples. The AFM data for surface rms roughness are presented in Table I as well. A small difference in absolute values of rms roughness obtained by GIXS and AFM measurements arises most probably as a consequence of different areas for the data averaging in these methods.

As follows from Eq. (3), the resonance diffuse scattering sheets observed in Fig. 3(a) indicate a strong vertical correlation of the roughness between the interfaces in the superlattice.^{15,20} Further detailed information about the interfacial roughness can be provided by the analysis of the size and shape of different RDS sheets. Figure 4 shows the detailed maps of the fifth and the eighth RDS sheets. They were measured for sample 1 along the miscut directions and perpendicular to it using the setup with analyzing slit. The maps measured in reverse directions (after azimuthal rotation of the sample by 180°) exhibited mirrored features, as expected. The maps in Figs. 3 and 4 are compressed in the q_z direction due to the different scales along the q_x and q_z axes.

First of all, the experimental maps in Fig. 4 exhibit very different q_x widths of the RDS sheets measured in AM and PM directions. This is an evidence for a strong anisotropy of lateral size of interfacial roughness (see Sec. II). A larger q_x width of RDS indicates a smaller lateral correlation length of

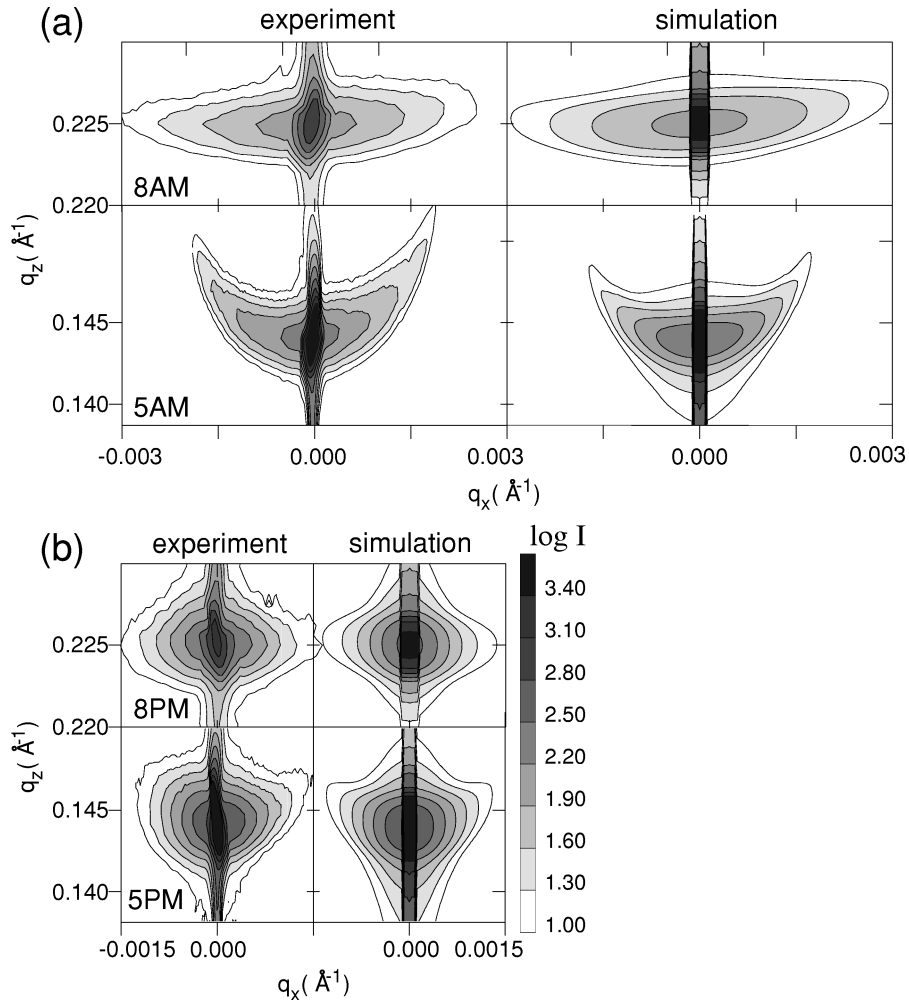


FIG. 4. Reciprocal space maps of the fifth and the eighth RDS sheets for sample 1. (a): 5AM, 8AM — results of x-ray measurements in the direction along miscut and corresponding simulations, (b): 5PM, 8PM — the same for direction perpendicular to miscut.

roughness in the direction along the miscut than perpendicular to it.

Another peculiarity of the RDS sheets in Fig. 4 is a small tilt in the $q_x q_z$ plane, or the asymmetry of the q_x sections of RDS with respect to the central specular reflection peak (Fig. 5). According to the theory described in Sec. II this kind of asymmetry of diffuse scattering is due to skew roughness inheritance by successive interfaces.

Both the anisotropy and asymmetry effects are observed for the other samples as well. The RDS maps for sample 2, 3, and 4 are presented in Fig. 6. The maps of the eighth RDS sheet for samples 3 and 4 are not shown because they do not provide any additional information.

In the first approximation the skew inheritance angle was measured as the tilt angle of RDS in the figures taking into account the difference in the scales of q_x and q_z . The following convention was used for the signs of skew inheritance. For AM direction the “+” sign was assigned to the skew angle when the roughness was inherited towards the step-flow direction, as taken from the literature¹⁶ and shown in Fig. 1. In Fig. 2(a) this positive direction coincides with $[110]$. For PM direction, where there is not such a clear criteria, the skew angle was assigned positive when the inheritance was inclined towards $[1\bar{1}0]$, see Fig. 2(b). The measured skew angle values were taken as starting param-

eters for computer simulations of RDS sheets.

The simulations of GIXS were performed according to Eq. (4) with the correlation function in the form (5). The fitted parameters were the lateral and vertical correlation lengths, the roughness exponent (jaggedness), and the skew angle of roughness inheritance (see Table II). An additional parameter was the relative height of *correlated* roughness. It was determined by comparing the intensities of measured GIXS with corresponding theoretical cross sections calculated using the total rms roughness. The ratio of these two values was nearly the same for samples 1–3, while for sample 4 GIXS was weak and the ratio was about 6 times less. This corresponded to about 2.5 times lower rms of correlated roughness in the sample 4 (see Fig. 5 and Table II).

The determination of roughness parameters from GIXS data is usually based on the fact that each of the parameters can be related to a particular feature of x-ray scattering pattern. For example, the lateral and vertical correlation lengths are inversely proportional to the extension of RDS in reciprocal space over q_x and q_z , respectively, while the value of the roughness exponent determines the descent of GIXS with q_x . Thus, different effects can be separated and preliminary estimations of the correlation lengths can be obtained measuring the half width of experimental RDS in the two directions. However, when GIXS measurements are implemented

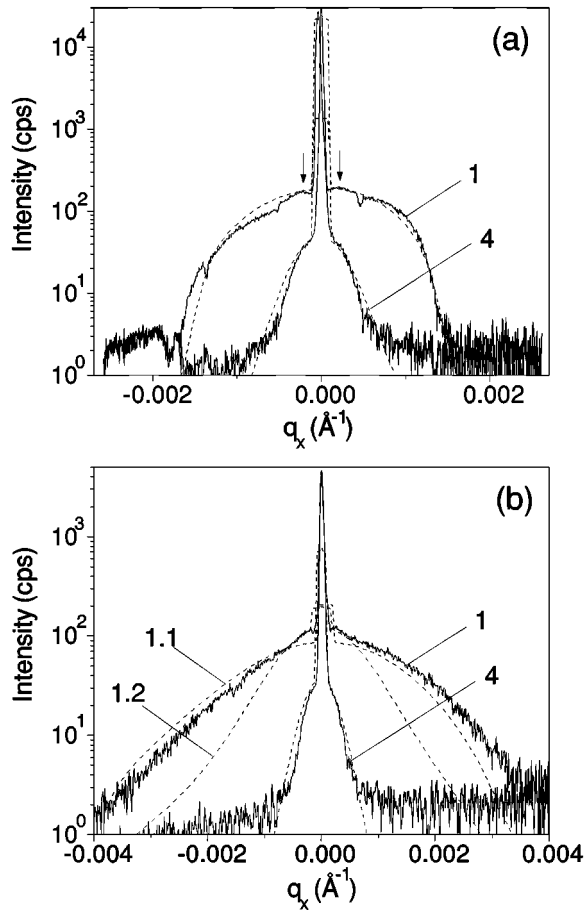


FIG. 5. Transverse scans through the fifth (a) and eighth (b) RDS sheets for sample 1 and sample 4 measured in the direction along miscut. Experimental and calculated curves are shown by solid and dotted lines, respectively. Dotted curves 1.1 and 1.2 correspond to simulations using lateral correlation lengths of 1000 Å and 2000 Å, respectively.

with the analyzing slit, their q_z resolution can turn out to be low, so that just the resolution itself, but not the correlation length determines the q_z half width of RDS. For example, estimating the vertical correlation length from the q_z -halfwidth of all experimental RDS sheets in Figs. 4, 6 one can find a very small vertical correlation length of about 500–900 Å in all the cases. That contradicts the presence of high-order RDS sheets on the map of Fig. 3(a), which indicates a higher vertical correlation of roughness. Thus, an improvement of the resolution is required. This fact was not taken into account in many previous studies, where only transverse scans providing sections of RDS at constant q_z were measured.

Using synchrotron radiation and the setup with analyzer crystal, the resolution was improved and the intrinsic width of the RDS sheets was measured. In Fig. 7 longitudinal and transverse scans taken from sample 1 in the AM direction across the fifth RDS sheet are presented. Here the measurements with conventional x-ray tube using an analyzing slit and with synchrotron radiation using an analyzer crystal are compared. The half width of the longitudinal scan obtained with the analyzer crystal $\Delta q_z = 10^{-3} \text{ \AA}^{-1}$ is two and a half times larger than the resolution of the setup. The accurate value of the vertical correlation length determined from this

curve amounts to 3000 Å. The vertical correlation lengths obtained from these high-resolution measurements are given in Table II for all the samples.

As one can see in Fig. 7(b), the transverse q_x scans also display a significant difference in their half width when measured either with an analyzing slit or with an analyzer crystal. The major reason for this is the influence of q_z resolution on the width of q_x sections. Since RDS sheets possess a crescent shape, the width of their lateral sections effectively increases when they are smeared due to low q_z resolution. Thus, the disregard of the q_z resolution of GIXS experiment can result in underestimated lateral correlation lengths.

In view of this argumentation, the calculated maps of RDS sheets were averaged taking into account experimental resolution in both q_x and q_z directions in order to compare them with experimental data and to obtain the correct values of lateral and vertical correlation lengths. The calculated transverse scans were obtained as sections of averaged calculated RDS sheets. These sections were compared to experimental transverse scans. Such a procedure gave lateral correlation lengths which agree with AFM data (see Sec. V).

The calculated averaged RDS sheets are shown for all the samples in Figs. 4, 6 along with the experimental data, and the fitted parameters are listed in Table II. The comparison of the q_x sections of calculated averaged maps with the experimental curves for samples 1 and 4 is presented in Fig. 5 and indicates their satisfactory agreement.

It should be mentioned that the fitting of the eighth RDS sheet of samples 1 and 2 indicates the presence of an additional component of interface roughness with a smaller lateral correlation length (see Figs. 4, 5, 6 and the lateral correlation length 2 in Table II). It could be attributed to an increase of the lateral correlation length with the superlattice growth, since the higher-order sheets are formed by diffuse scattering from a thicker probed surface layer.

The AFM images for all samples are displayed in Fig. 8. The surfaces of samples 1 and 3 show pronounced step bunches directed along $[1\bar{1}0]$ (Ga-terminated *A* steps). These bunches are restricted in their elongation in perpendicular $[110]$ direction by *B* steps, As terminated. Besides, the *A* steps of sample 1 [Fig. 8(a)] are smoother and more elongated, while for sample 3 [Fig. 8(c)] they are rougher, shorter, and resemble islands.

AFM images of sample 2 [Figs. 8(b), (f)] do not show any regular steps. However, on a larger length scale step bunches with a strong anisotropy of the shape can be observed [Fig. 8(f)]. For sample 4 GIXS indicates the smallest height of total and correlated roughness. This is also reflected in the AFM images [Fig. 8(d), (h)] which show a very small surface roughness of only 2.3 Å. Nevertheless, anisotropic relief, resembling steps, can be resolved [Fig. 8(d)], and on a larger length scale [Fig. 8(h)] some step bunches can be distinguished.

The lateral correlation lengths obtained by GIXS are indicated as bars on all AFM images of samples 1–4 in Fig. 8. It can be seen that x-ray and AFM data are in good agreement.

V. DISCUSSION

We have demonstrated that both the morphology of the vicinal surface of the substrate and the conditions of MBE

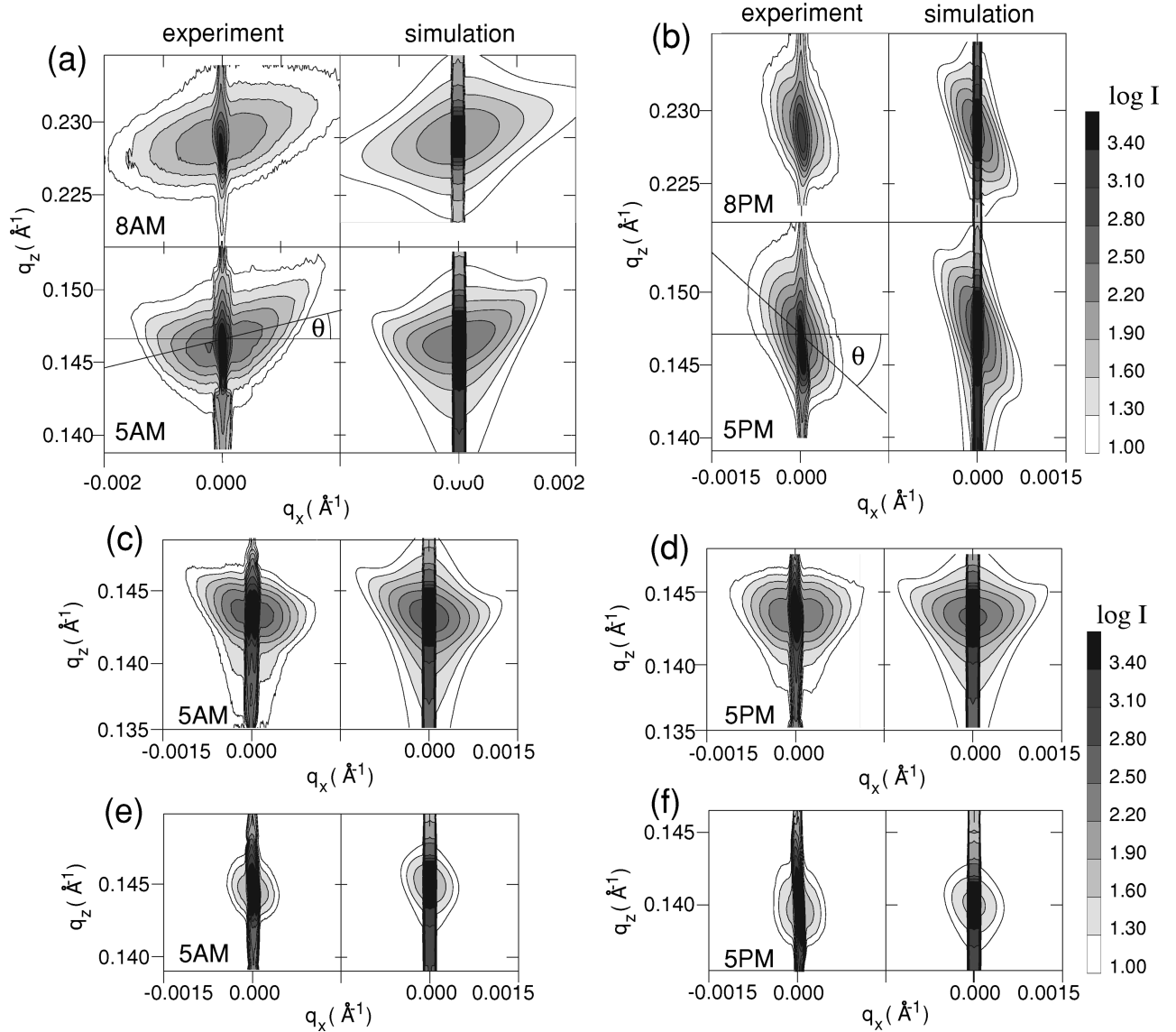


FIG. 6. Reciprocal space maps of the fifth and the eighth RDS sheets for sample 2 — (a),(b), and the fifth RDS sheet for sample 3 — (c),(d), and sample 4 — (e),(f). 5AM, 8AM — results of x-ray measurements in the direction along miscut and corresponding simulations; 5PM, 8PM — the same for direction perpendicular to miscut. θ is the angle of skew roughness inheritance.

growth influence the roughness of interfaces in AlAs/GaAs superlattices. In this section we will discuss this influence in more detail.

A. Roughness height

The magnitude of surface and interfacial roughness, found by GIXS measurements, is dependent on the quality of the initial surface prepared for superlattice growth. Since substrates are always roughened by pits and other defects formed during oxide desorption preceding superlattice growth,^{33,36} buffer layers are grown in order to improve the surface quality. It was shown previously^{33,36} that buffer layers grown at proper conditions (step flow mode) exhibit smooth surfaces with step arrays and large-scale lateral undulations (step bunches) after approximately 750 Å deposition. The increase in the buffer layer thickness can lead to smoother surfaces,^{36,45} although above 2000 Å a roughening can reappear. In consistency with these results, the increase

in the buffer layer thickness from 1000 Å to 2000 Å in our experiment results in smoother surfaces and interfaces of the superlattices, as proven by the reduced rms roughness of interfaces measured by GIXS and the surface rms roughness given by AFM (see Table I).

It is also known that a post-growth annealing at growth temperature can essentially influence the surface roughness of the buffer layer.^{33,35,36} The smoothing of surfaces due to surface diffusion was found by Smith *et al.*^{35,36} Annealed surfaces exhibited a lower step density and smoother large-scale undulations of roughness, although the monolayer steps edges became more irregular. Hey *et al.*³³ observed that the post-growth annealing at growth temperature (under arsenic flux) drastically changed the width distribution of as-grown step terraces. Prolonged annealing caused destruction of the regularity of as-grown step systems.

Our results confirm the smoothing of interfaces due to growth interruptions. As measured by both GIXS and AFM, the total rms roughness of surface and interfaces decreases

TABLE II. The interfacial roughness parameters, i.e., lateral and vertical correlation lengths, roughness exponents, skew inheritance angles, and relative correlated rms roughness obtained from simulations of GIXS maps. GIXS measurements are performed for samples 1–4 in two sample azimuth directions: along and perpendicular to miscut. Along the miscut direction some samples exhibit two components of roughness with different lateral and vertical correlation lengths marked as 1 and 2.

| Sample | 1 | | 2 | | 3 | | 4 | |
|---|-------|-------|-------|-------|-------|-------|-------|-------|
| Along miscut: | RDS-5 | RDS-8 | RDS-5 | RDS-8 | RDS-5 | RDS-8 | RDS-5 | RDS-8 |
| Lateral correlation length 1 (\AA), ± 250 | 2000 | 2000 | 2500 | 2500 | 4000 | 4000 | 5000 | 5000 |
| Lateral correlation length 2 (\AA), ± 250 | | 1000 | | 1000 | | | | |
| Roughness exponent (jaggedness), ± 0.1 | 0.8 | 0.8 | 0.8 | 0.7 | 0.9 | 0.9 | 0.9 | 0.9 |
| Vertical correlation length 1 (\AA), ± 250 | 3000 | 3000 | 1500 | 1500 | 2000 | 2000 | 1000 | 1000 |
| Vertical correlation length 2 (\AA), ± 250 | | 3000 | | 1000 | | | | |
| Skew inheritance angle ($^\circ$), ± 5 | -15 | -15 | -45 | -45 | 45 | 45 | 45 | 45 |
| Relative correlated rms roughness (%) | 100 | 100 | 100 | 100 | 100 | 100 | 40 | 40 |
| Perpendicular to miscut: | RDS-5 | RDS-8 | RDS-5 | RDS-8 | RDS-5 | RDS-8 | RDS-5 | RDS-8 |
| Lateral correlation length (\AA), ± 250 | 4000 | 4000 | 7000 | 7000 | 3500 | 3500 | 6000 | 6000 |
| Roughness exponent (jaggedness), ± 0.1 | 0.8 | 0.7 | 0.9 | 0.8 | 0.9 | 0.9 | 0.9 | 0.9 |
| Vertical correlation length (\AA), ± 250 | 3000 | 3000 | 1500 | 1500 | 2000 | 2000 | 1000 | 1000 |
| Skew inheritance angle ($^\circ$), ± 5 | 8 | 8 | 75 | 75 | 10 | 10 | 50 | 50 |
| Relative correlated rms roughness (%) | 100 | 100 | 100 | 100 | 100 | 100 | 40 | 40 |

when the superlattice is grown discontinuously on a multilayer buffer which is grown with growth interruptions (sample 4, Table I). The effect is even stronger for the vertically correlated component of interfacial roughness. The correlated roughness for a superlattice of the same sample 4 is 2.5 times smaller than in the other cases of a single buffer layer and continuous growth (Fig. 5 and Table II). It indicates that growth interruptions lead to a smoother surface and that the correlated roughness of interfaces in superlattices is to a greater extent a result of the morphology inheritance from the buffer layer than the total roughness. As we will see in the next section, the correlated roughness in the case of step-flow mode corresponds to the step bunches on the surface and interfaces of the superlattices.

B. Surface and interface morphology

For all the samples GIXS and AFM exhibit an anisotropy of the surface and interface morphology related to the miscut. The origin of this anisotropy is the stepped initial surface as the template for the superlattice growth. However, this characteristic feature can be strongly modified by different growth modes. The step-flow mode provides distinct step bunches whereas 2D nucleation provides islands, different in height and habitus, as confirmed by AFM images of sample 1 and 3 [Figs. 8(a), (c), (e), (g)], respectively. GIXS measurements also confirm this fact: the AM lateral correlation length is 2 times smaller than the PM length for sample 1 grown in step-flow mode, while both the correlation lengths are comparable for sample 3 grown in 2D nucleation mode (see Table II). Transitional mode of growth can preserve the anisotropy. AM lateral correlation length is nearly 3 times smaller than PM length for sample 2, although the steps are no longer clearly resolved on the surface [Figs. 8(b), (f)].

A further comparison of x-ray and AFM results reveals that the characteristic lateral correlation length, obtained from GIXS, corresponds with the size of the step bunches or islands, but not with the width of the terraces for single steps.

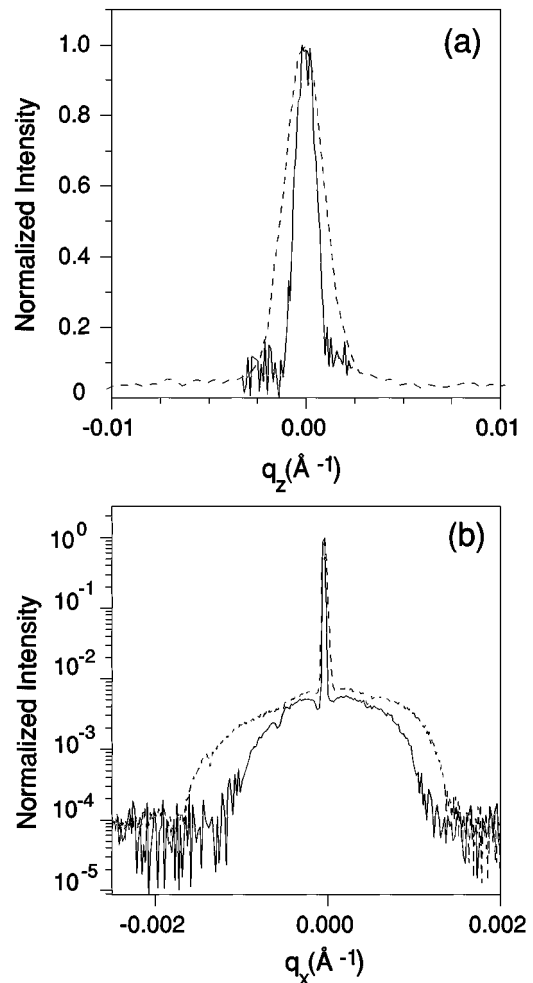


FIG. 7. Longitudinal (a) and transverse (b) scans through the fifth RDS sheet from sample 1 taken along the miscut direction on different experimental setups. Curves measured with a conventional x-ray tube and analyzing slit are shown by dotted lines. Results of synchrotron measurements using a crystal analyzer are shown by solid lines.

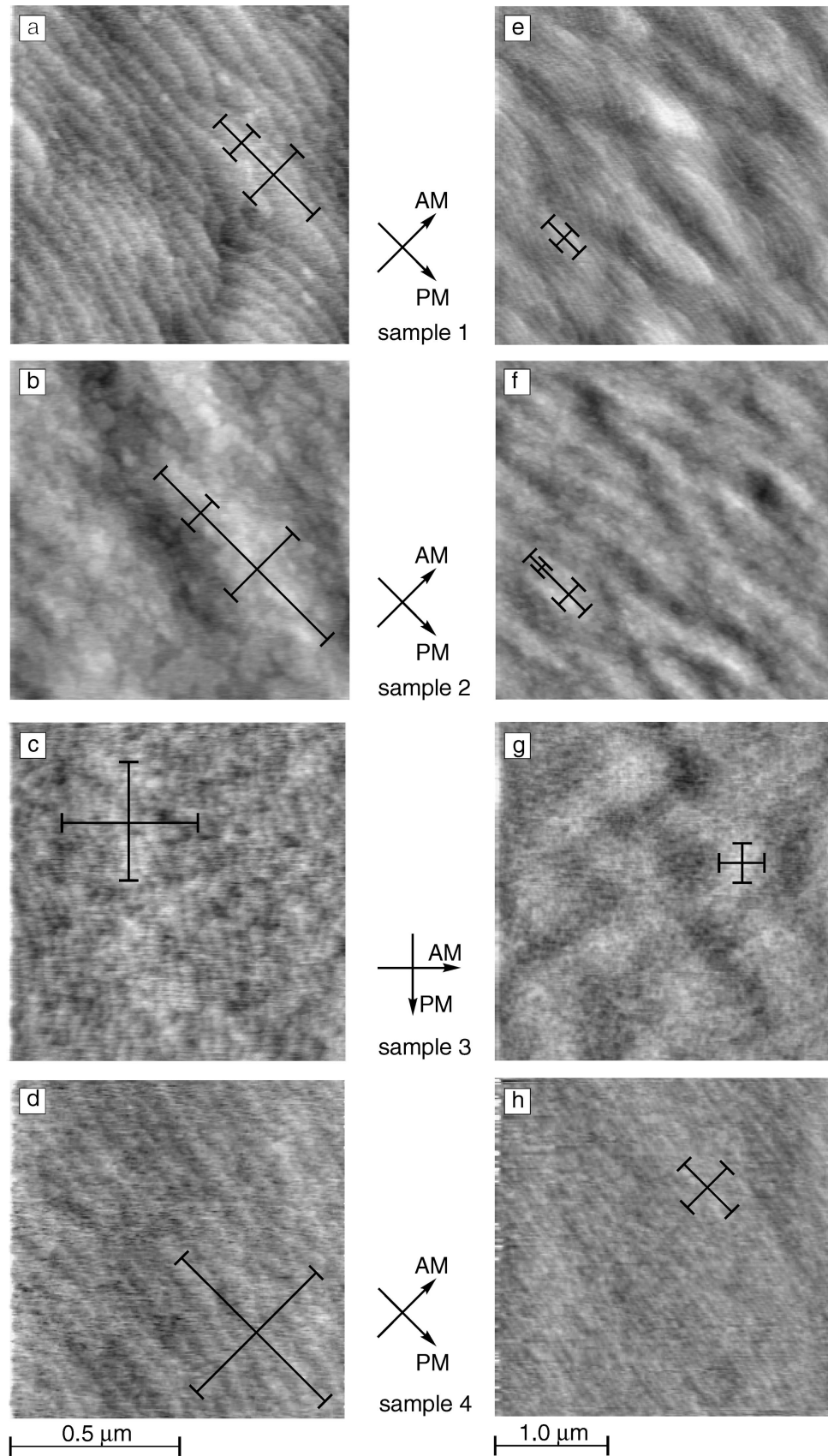


FIG. 8. AFM images of GaAs surface of samples 1–4 (subscribed in respective order). (a)–(d) Images of $1 \times 1 \mu\text{m}^2$ area; (e)–(h) images of $3 \times 3 \mu\text{m}^2$ area. The directions along the miscut and perpendicular to it are shown by arrows for each image. Bars on the images indicate lateral correlation lengths given by GIXS.

The lateral correlation lengths measured in the direction along the miscut, 2000–5000 Å, are much larger than the width of terraces calculated for the nominal miscut angle and the monostep height. The averaged terrace width is about 400 Å for the samples with a miscut angle of about 0.4° and the monosteps consisting of GaAs or AlAs bilayers with a height of about 2.8 Å.

Growth interruptions also strongly influence the surface and interface morphology. In line with the observations of lower step density³⁵ and formation of rather large terraces³³ at growth interruptions, our results show that discontinuous growth leads to interfacial roughness with a larger lateral correlation length in both along and perpendicular to miscut directions (see Table II). However, the vertical correlation length becomes smaller. We will discuss this fact in the next subsection. The growth interruptions also cause a stronger anisotropy of roughness due to the greater increase in the lateral correlation length perpendicular to the miscut direction, than along the miscut, as observed by GIXS (see Table II). This result is consistent with the observations by Smith *et al.*³⁵ that annealed surfaces show a larger step spacing and a longer size of steps in the direction perpendicular to miscut.

C. Roughness inheritance

In contrast to AFM, x-ray diffuse scattering also provides information about the roughness of buried interfaces and the correlation of the roughness between interfaces. The correlation of interfacial roughness in the vertical direction through the multilayer stack was strongly influenced by the mode of superlattice growth and the use of growth interruptions. The vertical correlation length was less than the thickness of the whole superlattice (about 4400 Å) for all the samples. The largest vertical correlation length of about 75% of the superlattice thickness was observed for sample 1 grown in the step-flow mode and without growth interruptions. A smaller length, about a half of superlattice thickness, was obtained for sample 3 grown in the 2D nucleation mode and also without growth interruptions. Growth interruptions significantly destroyed the vertical correlation of the interfacial roughness and resulted in the smallest vertical correlation length (about 25% of the superlattice thickness), as observed for samples 2 and 4. It is possible to conclude that continuous step-flow growth provides the best conditions for inheritance of interface morphology (step bunches) by successive interfaces, while the modification of the surface at growth interruption breaks this progression at each AlAs-on-GaAs interface and decreases the extent of vertical correlation of roughness.

For all the samples the inheritance of roughness by successive interfaces in superlattices occurred in an inclined direction with respect to the sample surface normal. As a consequence of the inclined inheritance of roughness, the RDS sheets are tilted (see Figs. 4 and 6 and Sec. II). The effect of the skew roughness inheritance was observed previously by other authors^{16,21} and was connected with a miscut of the substrate. The direction of skew inheritance was found to coincide with the direction of step flow on growing vicinal surfaces.⁴⁶ In our study we have found some different effects (see Figs. 4, 6 and Table II).

First, a strong component of skew roughness inheritance was also observed in the direction perpendicular to the miscut which together with a component along the miscut gave inheritance in some intermediate direction. This effect appeared due to the 120 s growth interruptions after each GaAs layer. For such samples, the PM component of roughness transfer was characterized by very large skew angles of 45°–75°.

Second, negative skew angles of roughness inheritance are found in the direction along the miscut. This means that the inclination of roughness transfer proceeds in the direction opposite to the direction of step flow. This effect is observed for sample 1 grown in the step-flow mode on thin buffer layer (the highest total, surface, and correlated rms roughness). The angle of negative transfer is small, but certainly above possible experimental errors. The perpendicular-to-miscut component of roughness inheritance for this sample is nearly zero. One possible explanation for the negative skew angle could be such a large lateral transfer of step bunches *in the positive direction* that they could pass nearly the whole lateral correlation length. If the surface relief is periodic, the cases of roughness transfer with large positive and small negative skew angles become equivalent. Some evidence of the relief periodicity is observed for sample 1 as peaks in diffuse scattering in Fig. 5 (shown by arrows).

However, the very large negative skew angle is observed for sample 2 grown on a similar rough surface to sample 1, but in a transitional growth mode [steps are not resolved on AFM image in Fig. 8(b)] and with growth interruptions. In addition, sample 2 exhibits the strongest component of inclined inheritance of roughness in the perpendicular-to-miscut direction. The latter effect means that the annealing breaks the symmetry between $[1\bar{1}0]$ and $[\bar{1}10]$ directions, which is otherwise preserved (the symmetry between $[110]$ and $[\bar{1}\bar{1}0]$ is broken by the miscut). To our knowledge, the only probable explanation for this effect could be a formation of some facets or roughness undulation with a preferred crystallographic orientation other than the miscut direction. This could happen as a result of surface diffusion during growth interruptions. An indirect confirmation to this fact are the observations of irregularly shaped step edges found by other authors^{33,35,34} on the surfaces of annealed or discontinuously grown samples. Finally, we would like to point out that further systematic investigations are necessary to provide a detailed model of the mechanisms that are responsible for skew roughness inheritance during epitaxial growth.

Our study, probably, exhausted the opportunities provided by laboratory x-ray equipment. The experiments which would be desirable—obtaining direct information on the shape of the correlation function using out-of-planes GIXS measurements over a very wide range of momentum transfers q_y ,^{17,47,48} or determining the atomic ordering within the roughness with GIXS near the grazing-incidence diffraction peaks,²⁶ both require either a wiggler or a third-generation synchrotron radiation source.

VI. SUMMARY

The surface and interfacial roughness in AlAs/GaAs superlattices grown by MBE on vicinal (001) GaAs substrates have been studied depending upon different growth modes,

growth interruptions, and substrate preparation. The two techniques applied to this study, the grazing-incidence x-ray scattering and the atomic force microscopy, have been shown to provide complementary information on the roughness.

The crucial parameter changing the morphology of surface and interfaces of the superlattices grown on the substrates with the same miscut angles was the growth mode. The samples grown in the step-flow mode exhibited step bunching on the surface and interfaces possessing a strong azimuthal *anisotropy*. According to this, the lateral correlation length of roughness measured in the direction along the miscut was smaller than perpendicular to it. On the other hand, the sample grown in two-dimensional nucleation mode exhibits no anisotropy of roughness.

It has been confirmed that surface and interfacial roughness of superlattices strongly depends on the substrate preparation. The rms height of roughness decreased and the lateral correlation length increased with the improvement of quality of the buffer layer surface. This proves that the interfaces of the superlattices inherited the substrate morphology.

A strong asymmetry of interfacial roughness inheritance has been observed via the asymmetry of GIXS. The theoretical analysis has shown that this can be due to either a skew roughness inheritance in multilayers or the steps at vicinal interfaces. In the former case each resonance sheet is tilted by the inclination angle, so that the sheets stay normal to the inheritance direction. In the latter case the whole GIXS pattern lines up along the crystallographic direction normal to terraces at the vicinal interfaces. For all our samples the GIXS asymmetry has been found to be due to the skew inheritance of roughness and no asymmetry due to the steps at vicinal interfaces was evident.

It has been shown that growth interruptions smooth the interfaces, but drastically destroy the roughness inheritance in superlattices. The correlation of interfacial roughness along the superlattice stack was much less for discontinu-

ously grown samples. The first observation, to our knowledge, of the inclination of roughness inheritance in the direction perpendicular to the miscut has been reported. Together with an inclination along the miscut it provided the inheritance in some intermediate direction. It has been suggested that surface diffusion during growth interruptions results in the formation of some facets or roughness undulations with a preferred crystallographic orientation. This breaks the symmetry and provides a possibility of skew inheritance in the direction other than the miscut one.

Another effect observed is the negative inclination angles of roughness inheritance measured in the direction along the miscut. This effect has been found for the superlattices grown on insufficiently smooth thin buffer layers. It was enhanced by growth interruptions at the transitional mode of growth. We suppose that in this case as well the inheritance is in the positive direction of the step flow, but with a large angle, so that the steps could pass the whole lateral correlation length.

It has been found that the 2D mapping of GIXS in the reciprocal space is urgently required for the characterization of roughness in multilayers. The q_x scans of GIXS used in many previous studies may be fitted by incorrect lateral correlation length of roughness, when the vertical intrinsic width of the resonance sheets of GIXS is unknown. The q_x scans drawn through the centers of the RDS sheet may not reveal the asymmetry caused by skew roughness inheritance.

ACKNOWLEDGMENTS

This work was supported by the Volkswagen Foundation, Federal Republic of Germany (Project No. 1/72439), and by "Deutsche Forschungsgemeinschaft" within the framework of Sfb 296. We are grateful to A. A. Chernov (Institute of Crystallography, Moscow) and H. Raidt (AG Röntgenbeugung) for valuable advice. One of us (S.A.S.) is also pleased to thank V. Holý (Masaryk University, Brno) and S. Sinha (Argonne National Laboratory) for stimulating discussions.

-
- *On leave from: Institute for Nuclear Problems, 11 Bobruiskaya St., Minsk 220050, Republic of Belarus.
- ¹S. K. Sinha, E. B. Sirota, S. Garoff, and H. B. Stanley, *Phys. Rev. B* **38**, 2297 (1988).
 - ²A. V. Andreev, A. G. Michette, and A. Renwick, *J. Mod. Opt.* **35**, 1667 (1988).
 - ³S. K. Sinha, *Physica B* **173**, 25 (1991).
 - ⁴T. A. Rabedeau *et al.*, *Appl. Phys. Lett.* **59**, 3422 (1991).
 - ⁵D. E. Savage *et al.*, *J. Appl. Phys.* **69**, 1411 (1991).
 - ⁶J. B. Kortright, *J. Appl. Phys.* **70**, 3620 (1991).
 - ⁷Y. H. Phang *et al.*, *Appl. Phys. Lett.* **60**, 2986 (1992).
 - ⁸X. Jiang, T. H. Metzger, and J. Peisl, *Appl. Phys. Lett.* **61**, 904 (1992).
 - ⁹Z. H. Ming *et al.*, *Phys. Rev. B* **47**, 16 373 (1993).
 - ¹⁰R. L. Headrick and J.-M. Baribeau, *Phys. Rev. B* **48**, 9174 (1993).
 - ¹¹E. Spiller, D. Stearns, and M. Krumrey, *J. Appl. Phys.* **74**, 107 (1993).
 - ¹²V. Holý *et al.*, *Phys. Rev. B* **47**, 15 896 (1993).
 - ¹³S. K. Sinha, *J. Phys. (France) III* **4**, 1543 (1994).
 - ¹⁴S. K. Sinha *et al.*, *Physica B* **198**, 72 (1994).
 - ¹⁵V. Holý and T. Baumbach, *Phys. Rev. B* **49**, 10 668 (1994).
 - ¹⁶Y. H. Phang *et al.*, *Phys. Rev. B* **50**, 14 435 (1994).
 - ¹⁷T. Salditt, T. H. Metzger, and J. Peisl, *Phys. Rev. Lett.* **73**, 2228 (1994).
 - ¹⁸D. K. G. de Boer, *Phys. Rev. B* **49**, 5817 (1994).
 - ¹⁹M. Tolan *et al.*, *J. Phys. D* **28**, A231 (1994).
 - ²⁰V. M. Kaganer, S. A. Stepanov, and R. Köhler, *Phys. Rev. B* **52**, 16 369 (1995).
 - ²¹R. L. Headrick, J.-M. Baribeau, and Y. E. Strausser, *Appl. Phys. Lett.* **66**, 96 (1995).
 - ²²C. Teichert *et al.*, *Appl. Phys. Lett.* **66**, 2346 (1995).
 - ²³J.-P. Schlomka *et al.*, *Phys. Rev. B* **51**, 2311 (1995).
 - ²⁴D. K. G. de Boer, A. J. G. Leenaers, and R. M. Wolf, *J. Phys. D* **28**, A227 (1995).
 - ²⁵B. Jenichen, S. A. Stepanov, B. Brar, and H. Kroemer, *J. Appl. Phys.* **79**, 120 (1996).
 - ²⁶S. A. Stepanov *et al.*, *Phys. Rev. B* **54**, 8150 (1996).
 - ²⁷J. Stettner *et al.*, *Phys. Rev. B* **53**, 1398 (1996).
 - ²⁸E. A. Kondrashkina *et al.*, in *IUCr XVII Collected Abstracts* (IUCr, Seattle, WA, 1996), p. 474.
 - ²⁹C. Giannini *et al.*, in *IUCr XVII Collected Abstracts* (IUCr, Seattle, WA, 1996), p. 465.
 - ³⁰B. Jenichen, R. Hey, M. Wassermeier, and K. Ploog, *Nuovo Cimento D* **19**, 429 (1997).

- ³¹L. G. Parratt, *Phys. Rev.* **95**, 359 (1954).
- ³²F. Abeles, *Ann. Phys. (Paris)* **3**, 504 (1948); **5**, 596 (1950).
- ³³R. Hey *et al.*, *J. Cryst. Growth* **154**, 1 (1995).
- ³⁴R. Hey *et al.*, *J. Cryst. Growth* **175/176**, 1167 (1997).
- ³⁵G. V. Smith *et al.*, *Appl. Phys. Lett.* **59**, 3282 (1991).
- ³⁶G. V. Smith *et al.*, *J. Cryst. Growth* **127**, 966 (1993).
- ³⁷M. Henzler, *Surf. Sci.* **73**, 240 (1978).
- ³⁸C. S. Lent and P. I. Cohen, *Surf. Sci.* **139**, 121 (1984).
- ³⁹P. R. Pukite, C. S. Lent, and P. I. Cohen, *Surf. Sci.* **161**, 39 (1985).
- ⁴⁰J. M. Pimbley and T. M. Lu, *Surf. Sci.* **159**, 169 (1985).
- ⁴¹J. Wollschläger, J. Falta, and M. Henzler, *Appl. Phys. A* **50**, 57 (1990).
- ⁴²M. Yoon *et al.*, *Phys. Rev. B* **49**, 16 702 (1994).
- ⁴³This choice is close to the self-affine model of roughness with $h=0.5$. On the other hand, assuming a periodic staircase, one can explain the periodic peaks in transverse scans of GIXS observed by Giannini *et al.* (Ref. 29).
- ⁴⁴E. A. Kondrashkina *et al.*, in *HASYLAB Annual Report (DESY, Hamburg, Germany, 1996)*, Vol. 1, pp. 484–485.
- ⁴⁵J. A. Dura, J. G. Pellegrino, and C. A. Richter, *Appl. Phys. Lett.* **69**, 1134 (1996).
- ⁴⁶M. Takeuchi *et al.*, *Jpn. J. Appl. Phys.* **34**, 4411 (1995).
- ⁴⁷T. Salditt *et al.*, *Europhys. Lett.* **32**, 331 (1995).
- ⁴⁸R. Paniago *et al.*, *Phys. Rev. B* **52**, 17 052 (1995).